Single crystal growth of FeRh from AuPb flux

Nikola Subotić, [1,2,3] Miwako Takahashi,[1] Takashi Mochiku,[4] Yoshitaka Matsushita,[4] Takanari Kashiwagi,[1] Osamu Takeuchi,[1] Hidemi Shigekawa,[1] and Kazuo Kadowaki[2]

[1]*Department of Pure and Applied Science, University of Tsukuba, 1-1-1 Tenoudai, Tsukuba, Ibaraki 305-8573, Japan*

[2]*Institute for Quantum Material Research (IQMR), 3441-19, Kurihara, Tsukuba, Ibaraki 305-0001, Japan*

[3]*Montenegrin Science Promotion Foundation (PRONA), Ul. Marka Radovic´a br. 149, 81000 Podgorica, Montenegro*

[4]*National Institute for Material Science (NIMS), 1-2-1 Sengen, Tsukuba, Ibaraki 305-0047, Japan*

The FeRh compound has been known for a long time as an itinerant magnet with a peculiar first-order antiferromagnetic (AFM)-to-ferromagnetic (FM) transition near room temperature. Although a lot of work has been done, the origin of the physical properties associated with the AFM ↔ FM transition is still an ongoing debate and needs deeper investigation using good single crystals. Here, we report on the single-crystal growth of FeRh from the AuPb flux and confirm it by x-ray crystallographic methods such as Laue diffraction, four-circle diffractometer measurements, and electron probe microanalyzer elemental analysis. The temperature dependence of magnetization in our single crystals below the AFM ↔ FM transition shows an anomalous cascadelike multiple transition behavior, which is obviously very different from the reported results previously. It is only such high-quality single crystals grown here that will pave the way for a comprehensive understanding of the longstanding issues of the FeRh compound.

I. INTRODUCTION

The intermetallic compound FeRh crystalizes into the CsCl (*Pm*-3*m*; B2 type) crystal structure [1]. Despite having a simple, high-symmetry crystal structure, FeRh exhibits complex magnetic, structural, thermodynamical, mechanical, and electrical behaviors. One of the most peculiar examples is the occurrence of the first-order ferromagnetic (FM)-to-

antiferromagnetic (AFM) transition ~350 K upon cooling [1]. Although the transition was reported more than 80 years ago [1], its origin is still under ongoing debate [2–9]. The transition is accompanied by the lattice expansion which varies from 0.3 to 1% depending on the sample preparation [6,7,10]. At first, the crystal structure change through the transition was reported to be like the α-γ transformation of Fe (magnetostructural transition) [1], while the later results stated that the crystal structure remains the same [10] (magnetoelastic transition). Due to the FM-AFM transition, giant magnetocaloric [11,12], elastocaloric [13], barocaloric [14], magnetostrictive [15], and magnetoresistive [16] effects occur. For the giant magnetocaloric effect, the entropy change is moderate, but the adiabatic temperature change holds the highest record value among all known room-temperature magnetocaloric materials [17]. Also, the transition exhibits a temperature memory effect [18]. Moreover, it was recently shown that the FeRh alloy doped with Ni exhibits a strikingly high value of the Thomson coefficient due to the steep change of the Seebeck coefficient during the transition [19], again, the highest value among all known materials near room temperature. Furthermore, FeRh has been reported to exhibit a topological Hall effect that is protected by a nonzero Berry phase in real space [20]. Additionally, the magnetic structure of the AFM phase is reported to be a so-called G-type structure, which has the DO3, Fe_3Al-type symmetry (*Fm*-3*m*), known as the symmetry of the atomic order in the Heusler alloy Cu_2MnAl, which is favorable for the formation of topological states [21]. These properties make the FeRh compound uniquely intriguing and its application broad, such as magnetic refrigeration [14,22–24], heat-assisted magnetic recording [25,26], multiferroic devices [27,28], AFM memory [29,30], micromachine and shape memory devices, and medicine [6].

Although FeRh is such an attractive material with many peculiar physical properties, it appears that the binary phase diagram has not been established well [31]. First, according to Swartzendruber [31], it is not known at which temperature the FeRh alloy melts for almost all ranges of the composition. Second, the order-disorder transition temperature is also not exactly known. The high-temperature disordered phase is often referred to as the γ phase, which crystalizes into the face-centered cubic (fcc) crystal structure (the same as Rh and γ Fe), while the low-temperature ordered phase (the phase of interest) has a CsCl-type ordered structure that forms directly from the γ phase through the order-disorder transition [31]. The ordered phase undergoes a usual second-order paramagnetic (PM)-to-FM (which is often referred to as the α' phase in the literature) transition ~400 °C at equiatomic composition. As the α' phase is further cooled, it transforms into an AFM phase referred to as the α'' phase

without accompanying crystal structural change.

The usual sample preparation process is, first, melting at a temperature above $T_m \sim 1600$ °C, followed by long-term annealing at a temperature below the order-disorder transition between fcc and CsCl-type ordered structure (~1300 °C [31]) to reduce the volume fraction of the γ phase to a negligible amount. However, recent tenacious and beautiful work [32–35] demonstrated the opposite: the volume fraction of the γ phase can be as high as 14%, even though the samples were annealed for 2 weeks [33]. Moreover, it was observed that the microstructure is responsible for the drastic change of the AFM-FM transition temperature, not the composition of α' as previously thought [6,7,33]. This is a clear indication that the binary phase diagram Fe-Rh [7,31], which was constructed without considering the microstructure effect, is not adequate (that might be the reason why the binary phase diagram FeRh was shrouded in mystery for a long time in the first place). Accordingly, the physical properties of FeRh known so far in the literature turn out to be mixed alloy properties of two phases, ordered CsCl type, and the γ phase. Therefore, the intrinsic properties of the single phase are still under the cover of a dark veil of mystery, and one must be prudent enough to understand how physical, chemical, and thermodynamic properties of FeRh are related to the presence of foreign phases, for example, the γ phase [32–35], or the degree of disorder such as vacancies [10] or antisite doping. Answers to such questions could only be provided by examining high-quality single crystals and comparing the results with their polycrystal/polyphase counterparts, as suggested in Ref. [7]. In the literature, there is a report on the single-crystal growth of the FeRh compound along with the neutron diffraction and the Mössbauer study [36,37]. However, it is not clearly described how the formation of the γ phase was avoided in their crystal growth process only by annealing the melt-quenched FeRh at 1200 °C for a day or so [37], whose process in principle is the same as the one described in the aforementioned work [32–35].

To shed light on this interesting issue, we have recently developed an approach to prepare single-phase and single-crystal FeRh using AuPb flux. The crystal habits of FeRh, obtained from the growth attempts described in this paper, are platelike (up to 200 × 300 ×10 μm), cubic (up to 400 × 400 × 400 μm), and needlelike (up to 100 × 100 × 1500 μm). The quality of single crystals was examined by x-ray diffraction measurements and its composition by electron probe microanalyzer (EPMA) measurements. To further characterize the physical properties of our single crystals, the temperature dependence of magnetization was measured.

II. EXPERIMENTAL METHODS

A. Preliminary investigation

An AuPb flux was chosen for the single-crystal growth of FeRh for several reasons. First, it was noted that, during the crystal growth of $RhPb_2$ [38,39], the Fe crucible reacts with the RhPb melt, making Pb a suitable choice as a flux. Second, from the rich Pb part at a higher temperature of the ternary phase diagram Au-Pb-Rh, $AuPb_4Rh_5$ crystals tend to grow at the surface of the boule, making the extraction of the crystals easier [40]. Third, the solubility of Fe in the Au can reach up to 74 at. % at 1173 °C [41], which could promote the crystal growth of FeRh. Last, the melting temperature of the AuPb alloy can be as low as 212 °C for a Pb concentration of 85 at. % [42], clearly indicating that the melting temperature of FeRh could be lowered well below the order-disorder transition, avoiding the formation of the γ phase. Raw materials of Au and Pb were 99.9% purity in shots, while Rh and Fe were 99.9% purity in powder form (300 mesh), purchased from Furuuchi Chemical Co, Japan.

Before the crystal growth, as a preliminary test procedure, a corresponding amount of the material was melted in an evacuated quartz tube by the flame torch to observe the distribution of Fe inside the boule and to estimate the melting temperatures. It was noted, for a higher concentration of Fe than Rh, a higher degree of crystal precipitation was observed at the surface of the boule. After the flame torch treatment, for all melting experiments, the melted ingot was put into another evacuated quartz tube that was heat treated at various temperature profiles depending on the initial composition.

Due to the possibility of precipitation of FeRh crystals at the surface of the boule, an infrared mirror furnace [38,39] was used for the preliminary melting experiment because the surface of the boule during the growth can be monitored in detail with a camera. The initial composition of the preliminary melting experiment was Au : Fe : Pb : Rh = 2:2:4:1. An additional reason why Fe : Rh = 2:1 was chosen is to see if it is possible to grow completely ordered FeRh crystals in the Fe-rich side of the phase diagram. As expected, at higher temperatures, the precipitation of the edge of a cube from the melt was observed. As the temperature decreased, the cube dissolved. The crystal that was formed at the upper part of the boule at a higher temperature was probably an Fe-rich compound since the upper part of the boule was magnetic. At the lower part of the boule, after the melting experiment, the formation of $AuPb_2Rh_2$ was observed.

B. Compositions investigated and temperature profiles

The preliminary melting experiment provided crucial information: For the investigated ratio, at higher temperatures, the Fe compound, possibly FeRh, forms, and as the temperature is decreased, the formation of $AuPb_2Rh_2$ becomes more favorable. Thus, to avoid the formation of $AuPb_2Rh_2$ for the 2:2:4:1 ratio, the growth temperature should be >800 °C, the approximate melting temperature of $AuPb_2Rh_2$ [40]. In addition, FeRh : $AuPb_2$ = 1:x should be explored as well since useful information could be obtained and the formation of $AuPb_2Rh_2$ could be suppressed. In Table I, the investigated compositions are summarized. The prepared quartz tubes were put in a regular muffle furnace with a programable temperature profile. As shown later, the growth is seriously affected by how the quartz tube is placed in the furnace. In Fig. 1, the temperature profiles for A, B, and C melting experiments are shown.

III. RESULTS

A. Au:Fe:Pb:Rh = 2:2:4:1 ratio

The results of batch A are shown in Fig. 2. The grown boule contained three parts. The upper part, which was rich in Fe; the lower part, mostly $AuPb_2$ flux; and the bridgelike structure connecting the upper part of the boule with the lower one. A possible reason for this kind of boule structure may be that the evaporated Pb could not pass through the Fe-rich part of the boule, resulting in the separation of the upper part of the boule from the lower as the pressure of the Pb vapor increased.

The surface of the upper part of the boule contained a mixture of hexagonal $AuPb_2Rh_2$ crystals and FeRh. Going deeper inside the upper part of the boule, the formation of FeRh becomes more favorable. Due to the high density of nucleation, the intergrowth of FeRh crystals frequently occurs, resulting in interesting shapes and morphology [Fig. 3(a)]. Moreover, in some cases, the layer growth of the FeRh crystal, with clear terraces and edges, can be seen by scanning electron microscopy (SEM) [Fig. 3(b)]. The size of the crystals here varies from 10 to 50 μm. It is interesting to note that, if the dimensions of the crystal are in this range, it is easy to separate them by applying a small amount of force, while the opposite is true for crystals having a much smaller size.

In the middle part of the boule in Fig. 2, at its surface as well as inside, crystal formation is observed. Since the FeRh : AuPb ratio is smaller, the nucleation density is also smaller, resulting in cubiclike crystal habits with few intergrowths happening. At

the surface, triangular and platelike crystals could be observed. In this part, mostly FeRh crystals grow. The lower part of the boule contained only a few FeRh crystals with no intergrowth. The crystals shown in Fig. 2 tend to grow on the surface and have a platelike habit. Like the upper part of the boule, the growth of $AuPb_2Rh_2$ crystals with a hexagonal crystal habit was observed. It can be observed that AuPb flux plays an important role in the crystal formation of FeRh.

B. Au:Fe:Pb:Rh = 2:1:4:1 and Au:Fe:Pb:Rh = 4:1:8:1 ratios

The results of batch B_2 are shown in Fig. 4. Compared with batch A, the quartz tube was placed horizontally, as shown in Fig. 4(a). One part of the surface of the boule is shown in Fig. 4(b). The precipitation, bulk, and platelike and needlelike crystals were observed. In Fig. 4(c), some of the crystals extracted from the surface part of the boule are shown. As before, the crystals have been extracted from the flux by using diluted nitric acid. Due to the proximity of the growing crystals to each other, seldom intergrowth is observed. In Fig. 4(d), the needlelike crystals up to 1.5 mm in length are shown. Those crystals were extracted from the middle part of the boule. In Fig. 4(e), the extracted crystals from the bottom part of the boule are shown. The intergrowth compared with the single-crystal growth becomes more favorable.

Batches B_1 and C_2 yielded crystals with clear crystal habit, mostly platelike and cubiclike, forming at the surface of the boule, but the size is significantly different from the previous batches. Instead, crystal sizes with dimensions of $50 \times 50 \times 50$ μm for cubic shaped ones and $100 \times 100 \times 10$ μm for platelike ones were found. Batch C_1 did not yield any FeRh crystals except the ones formed due to the quenching process, as shown in Fig. 4(b).

C. EPMA and XRD analysis

The quality of the single crystal was evaluated by x-ray diffraction, and the results are shown in Fig. 5. The x-ray transmission Laue diffraction pattern of the single crystal is shown in Fig. 5(a), and the backscattering electron image of the single crystal with a thin rectangular shape of $300 \times 200 \times 20$ μm in size is shown in Fig. 5(b), on which the diffraction experiment was done. Figure 5(c) shows the ω-scan rocking curve of the 110 Bragg reflection measured using a four-circle diffractometer (AFC-7R, Rigaku with Mo $K\alpha$ radiation). The measured crystal is cubic in shape with dimensions of $25 \times 25 \times 25$ μm. This crystal was extracted from batch A, from the middle part of the boule. The peak profile was

well fitted with a Lorentz function, and the full width at half maximum (FWHM) was 0.26°. The FWHM is almost the same as the resolution width, indicating that the quality of the sample is quite high. With this sample, structural analysis has been done with 281 reflections whose lattice spacing was $d < 0.625$ A. The result confirmed that the crystal structure is in a completely ordered phase of the CsCl type with the lattice parameter being $a = 2.9891(7)$ Å. The value coincides with the reported value for the AFM phase of the Fe-Rh alloy [32]. The Laue pattern certainly has a fourfold symmetry, suggesting that the flat plane of the single crystal is the (100) plane. The crystal has a well-developed rectangular shape with shiny surfaces, which intersect each other at a right angle, as expected from cubic symmetry. This crystal is the same one shown in Fig. 2(j). The data reduction yielded $R_{\text{int}} = 0.071$, indicating that the absorption correction was adequate.

In Table II, the results of the EPMA analysis are given, and in Fig. 6, the SEM images of the measured samples are shown. The acceleration voltage was 20 keV, and the beam spot diameter was as small as 1 μm. The averaged values of Fe and Rh concentrations are shown along with the calculated standard deviation. The measured spots were chosen carefully and measured repeatedly 10–14 times, and the results were averaged to obtain the most reliable data. The criterion for the measurement spot was a flat surface without AuPb flux and carbon tape residue. The average values are ~50% for both Fe and Rh concentrations.

D. Magnetization

In Fig. 7, the temperature dependence of magnetization measured from 10 to 400 K in 1 T magnetic field applied to the [1,0,0] direction is shown. The measured sample is sample No. 1 listed in Table II. First, the temperature was set to 10 K, and then a magnetic field of 1 T was applied. As shown in Fig. 7, the temperature dependence shows two anomalous kink behaviors. The minimum is reached ~130 K, while the change of the slope can be found at 284 K [field cooling (FC)] and 301 K [field warming (FW)] within the so-called AFM phase. Furthermore, it is interesting to point out that significant temperature hysteresis can be observed in a wide temperature range. The saturation magnetization above $T_{\text{FM}\leftrightarrow\text{AFM}}$ is 178 emu/g, which corresponds to 5.04 μ_B per FeRh molecule, while at lower temperatures, it is 66 emu/g, corresponding to 1.88 μ_B. All such anomalous magnetization behaviors cannot be explained by the simple AFM ordered state as previously considered [6,7] but may suggest

the consecutive occurrence of at least two magnetic phases.

IV. DISCUSSION

The results of batch A might seem chaotic, but several important things were noticed. First, obvious phase separation happens. Fe tends to migrate to the surface of the boule, modifying the local composition. Second, the surface of the boule plays an important role in the formation of the clear crystal habit of FeRh with no intergrowth in contrast with the crystals extracted from the inner and upper parts of the boule. Moreover, the FeRh : AuPb flux ratio affects the crystal growth as well. This becomes obvious by comparing the surfaces of the upper, middle, and lower parts of the boule. On the surface lower part of the boule, only one FeRh single crystal can be observed, which is an ideal condition for growing big-sized crystals. Third, even though the ratio of Fe : Rh at the upper part of the boule is at least two times bigger, the formation of Fe-doped FeRh crystals is not observed. This observation strongly suggests that the ordered FeRh phase line of Fe : Rh = 1:1 may exist in the ternary phase diagram. The line might have also existed in the binary phase diagram, but due to the low diffusion of the solid, the separation may not occur.

To reproduce the crystal growth condition that occurred on the surface of the lower part of the boule, the quartz tube was placed horizontally (B and C melting experiments), the same amounts of Fe and Rh were used, and the amount of the $AuPb_2$ flux was increased in the case of the C melting experiment. The results, as shown, are much improved from the crystal growth point of view. Needlelike, platelike, and bulklike crystals could be observed, being larger in size than the previous melting experiment A. This is concrete evidence that, for high-quality and bigger size crystal growth, the larger surface of the boule is crucial, which might be a unique feature of AuPb flux [40]. Another important point is that the phase separation is significantly reduced, allowing crystals to grow in all regions of the grown boule.

Combining the results of the melting experiments, a rough estimate can be made at which FeRh regions can form in the quaternary phase diagram of Au-Fe-Rh-Pb. The melting temperature of FeRh for 2:1:4:1 and 4:1:8:1 ratios are ~850 and 580 °C, respectively, since only small cubiclike crystals have been grown. Also, for batch B_2, FeRh crystals form due to quenching. Accordingly, the ratios between 2:1:4:1 and 4:1:8:1 should also result in FeRh formation. Therefore, it can be concluded that FeRh can be grown in a surprisingly wide temperature range and AuPb flux concentration. This is the starting point of further

investigation, i.e., optimization of FeRh crystal growth. Regarding the Au-rich part of the phase diagram, one can ask if FeRh crystals or maybe some new compound forms. For example, it was noted from the 4:1:8:1 ratio that, at lower temperatures, Au-doped $RhPb_4$ crystals form.

Another intriguing question to ask is to what extent Au has a dominant role in the formation of the single-phase, single-crystal FeRh. Since the phase diagrams of the binary compounds FeX, with X = Ni, Ir, Pd, Pt, etc., are surprisingly very similar to the case of FeRh, the answer to this question can be obtained rather directly by growing FeX compounds and investigating whether FeX compounds can be formed out of Au-Pb flux or not. As can be seen, by EPMA measurements, Au was not detected in our single crystals of FeRh within our detection level of 1 at. %, whereas Au-doping in FeRh up to several at. % of Au has been reported to strongly suppress and decrease $T_{FM\leftrightarrow AFM}$ [7,43,44]. These latter results certainly contradict our results. However, to compromise and solve this inconsistency, it is possible to think that only the doping of the γ phase with Au may occur but not in the α' phase since our sample is a pure single crystal with the α' phase only. This could explain the absence of Au in our samples.

The preliminary magnetization study has been carried out by using a SQUID magnetometer (Quantum Design MMPMS) on a few single crystals obtained from different batches grown in different ampoules. All the results are con- sistent and in very good agreement, but they are very different from the ones reported previously [6,7], as was pointed out earlier in Fig. 7 as an example of apparently different be- haviors. It may not be a surprise since our sample does not contain the γ phase, which on the contrary remained in the samples used in the previous works as the primary impurity phase, which seems to be extremely difficult to remove by thermodynamical procedures only.

The most striking difference in the magnetization behavior shown in Fig. 7 is the temperature dependence of magnetization: It exhibits strange two-kink behaviors at T_{AF1} = 130 K and T_{AF2} = 302 K for the heating process, while T_{AF1} smears out and T_{AF2} = 284 K for the cooling process. The temperature dependence of magnetization strongly indicates the existence of some additional magnetic phase transitions in the AFM phase, suggesting nontrivial complicated ordered structures. Although the detailed mechanism of such complicated magnetic phases remains unknown and needs deeper study in both experimental and theoretical works to fully understand them, it may be worthwhile pointing out that the

Rh moment may play an important role, as discussed in the mechanism of the AFM ↔ FM phase transition, where the presence or absence of the magnetic moment of Rh in the AFM phase is crucial. If Rh carries a magnetic moment, then the AFM structure cannot be simple, resulting in the more complicated structure being under ongoing debate [45]. Finally, we would like to comment on the possible explanation for why our results are so different from previous ones. The reason may be due to the pressure effect which stabilizes the AFM phase [46] through the remaining γ phase [33] as an impurity phase with different lattice parameters. This can be easily verified by measuring the magnetization of our single crystals of FeRh under pressure. The temperature dependence of magnetization shown in Fig. 7 indicates a kink at ~130 K and increases as the temperature decreases and finally saturates at low temperatures. This discovery strongly suggests that, <130 K, a new magnetic phase becomes stable. This should be confirmed further by other experimental techniques such as neutron diffraction. Growing crystals that are suitable for neutron diffraction is underway. It is certainly a great challenge since hopper crystal growth was observed [Fig. 4(e)]. Another intriguing point is the magnetic saturation moment value, which corresponds to 5 μ_B/f.u. of FeRh, indicating a considerably larger value than all values reported previously [6,7], except in Ref. [47]. All these facts cast serious intriguing questions about how the phase transformation $T_{FM\leftrightarrow AFM}$ can occur, what sort of magnetically ordered phases emerge in the single-phase single crystals, and what kind of mechanism is driving them. Considering the hypersensitivity of the physical properties of FeRh to doping and impurities, all kinds of measurements must be redone to establish intrinsic properties of a unique and rare system of FeRh using newly grown single crystals, which is currently in progress.

V. CONCLUSIONS

Single crystals of a famous and peculiar FeRh compound have been successfully grown from the unique AuPb flux. The method is surprisingly simple and elegant. Furthermore, the results are very transparent and reproducible, as shown above. The choice of the AuPb flux may be unorthodox, but the obtained single crystals are indeed pure and single-phase single crystals without any impurities within the limit of the detection level, as confirmed by x-ray single-crystal analysis as well as EPMA measurements. This widely opens the possibility to thoroughly reinvestigate the properties of FeRh, whose measurements have been done on unexpectedly impure materials in previous studies, and to deeply reconsider the fundamental

properties of pure FeRh, especially on the mechanism of the AFM ↔ FM phase transition as well as the newly emerging complicated magnetic phases. As shown in Fig. 7 in magnetization measurements as an example, the results are strikingly different from the previous ones. More detailed results on magnetic, transport, and thermodynamical measurements exhibiting unique and unprecedented properties are in progress and will be reported separately. Furthermore, our single crystals will provide an excellent opportunity to explore how physical, chemical, and metallurgical properties are affected by impurities, foreign atoms, vacancies, etc. Finally, AuPb flux might be useful for growing single crystals from other systems similar to Fe-Rh, such as FePt, FePd, FeIr, FeCo, FeNi, FeCr, and FeV, which is likely to spark further research.

ACKNOWLEDGMENTS

The corresponding author would like to thank Abdou Hassanien and Kaveh Delfanazari for their kind support and useful suggestions. Also, the corresponding author would like to thank Ministry of Education, Culture, Sports, Science and Technology (MEXT) for the financial support as a MEXT scholarship student. This paper is supported by the CROSS lab and is part of a research proposal: Magnetic and crystal structure analysis of FeRh single crystals, Proposal No. 2023B0151.

[1] M. Fallot, Ann. Phys. **11**, 291 (1938).

[2] V. L. Moruzzi and P. M. Marcus, Phys. Rev.B **46**, 2864 (1992).

[3] R. Y. Gu and V. P. Antropov, Phys. Rev. B **72**, 012403 (2005).

[4] M. E. Gruner, E. Hoffmann, and P. Entel, Phys. Rev. B **67**, 064415 (2003).

[5] S. O. Mariager, F. Pressacco, G. Ingold, A. Caviezel, E. Möhr- Vorobeva, P. Beaud, S. L. Johnson, C. J. Milne, E. Mancini, S. Moyerman *et al.*, Phys. Rev. Lett. **108**, 087201 (2012).

[6] R. R. Gimaev, A. A. Vaulin, A. F. Gubkin, and V. I. Zverev, Phys. Met. Mettalogr. **121**, 823 (2020).

[7] L. H. Lewis, C. H. Marrows, and S. Langridge, J. Phy. D **49**, 323002 (2016).

[8] J. S. Kouvel, J. Appl. Phys. **37**, 1257 (1966).

[9] P. Tu, A. J. Heeger, J. S. Kouvel, and J. B. Comly, J. Appl. Phys. **40**, 1368 (1969).

[10] L. Muldawer and F. Debergevin, J. Chem. Phys. **35**, 1904 (1961).

[11] S. A. Nikitin, G. Myalikgulyev, A. M. Tishin, M. P. Annaorazov, K. A. Asatryan, and A.

L. Tyurin, Phys. Lett. **148**, 363 (1990).

[12] M. P. Annaorazov, K. A. Asatryan, G. Myalikgulyev, S. A. Nikitin, A. M. Tishin, and A. L. Tyurin, Cryogenics **32**, 867 (1992).

[13] S. A. Nikitin, G. Myalikgulyev, M. P. Annaorazov, A. L. Tyurin, R. W. Myndyev, and S. A. Akopyan, Phys. Lett. **171**, 234 (1992).

[14] E. Stern-Taulats, A. Planes, P. Lloveras, M. Barrio, J. L. Tamarit, S. Pramanick, S. Majumdar, C. Frontera, and L. Mañosa, Phys. Rev.B **89**, 214105 (2014).

[15] M. R. Ibarra and P. A. Algarabel, Phys. Rev.B **50**, 4196 (1994).

[16] P. A. Algarabel, M. R. Ibarra, C. Marquina, A. Del Moral, J. Galibert, M. Iqbal, and S. Askenazy, Appl. Phys. Lett. **66**, 3061 (1995).

[17] N. A. Zarkevich and V. I. Zverev, Crystals **10**, 815 (2020).

[18] Y. Feng, T. Fukuda, and T. Kakeshita, Intermetallics **36**, 57 (2013).

[19] R. Modak, M. Murata, D. Hou, A. Miura, R. Iguchi, B. Xu, R. Guo, J. Shiomi, Y. Sakuraba, and K. Uchida, Appl. Phys. Rev. **9**, 011414 (2022).

[20] S. Zhang, S. Xia, Q. Cao, D. Wang, R. Liu, and Y. Du, Appl. Phys. Lett. **115**, 022404 (2019).

[21] K. Manna, Y. Sun, L. Muechler, J. Kübler, and C. Felser, Nat. Rev. Mater. **3**, 244 (2018).

[22] A. Chirkova, K. P. Skokov, L. Schultz, N. V. Baranov, O. Gutfleisch, and T. G. Woodcock, Acta Mater. **106**, 15 (2016).

[23] E. Stern-Taulats, T. Castán, A. Planes, L. H. Lewis, R. Barua, S. Pramanick, S. Majumdar, and L. Mañosa, Phys. Rev. B **95**, 104424 (2017).

[24] M. Manekar and S. B. Roy, J. Phys. D **41**, 192004 (2008).

[25] J. U. Thiele, S. Maat, and E. E. Fullerton, Appl. Phys. Lett. **82**, 2859 (2003).

[26] P. W. Huang and R. H. Victora, IEEE Trans. Magn. **50**, 1 (2014).

[27] R. O. Cherifi, V. Ivanovskaya, L. C. Phillips, A. Zobelli, I. C. Infante, E. Jacquet, V. Garcia, S. Fusil, P. R. Briddon, N. Guiblin *et al.*, Nat. Mater. **13**, 345 (2014).

[28] S. P. Bennett, A. T. Wong, A. Glavic, A. Herklotz, C. Urban, I. Valmianski, M. D. Biegalski, H. M. Christen, T. Z. Ward, and V. Lauter, Sci. Rep. **6**, 22708 (2016).

[29] T. Moriyama, N. Matsuzaki, K.-J. Kim, I. Suzuki, T. Taniyama, and T. Ono, Appl. Phys. Lett. **107**, 122403 (2015).

[30] X. Marti, I. Fina, C. Frontera, J. Liu, P. Wadley, Q. He, R. J. Paull, J. D. Clarkson, J. Kudrnovský, I. Turek *et al.*, Nat. Mater. **13**, 367 (2014).

[31] L. J. Swartzendruber, Bull. Alloy Phase Diagr. **5**, 456 (1984).

[32] C. F. Sánchez-Valdés, R. R. Gimaev, M. López-Cruz, J. L. Sánchez Llamazares, V. I. Zverev, A. M. Tishin, A. M. G. Carvalho, D. J. M. Aguiar, Y. Mudryk, and V. K. Pecharsky,
J. Magn. Magn. Mater. **498**, 166130 (2020).

[33] A. Chirkova, F. Bittner, K. Nenkov, N. V. Baranov, L. Schultz,
K. Nielsch, and T. G. Woodcock, Acta Mater. **131**, 31 (2017).

[34] A. M. Chirkova, K. P. Skokov, Y. Skourski, F. Scheibel, A.
Y. Karpenkov, A. S. Volegov, N. V. Baranov, K. Nielsch, L. Schultz, K.-H. Müller *et al.*,
Phys. Rev. Mater. **5**, 064412 (2021).

[35] A. S. Komlev, D. Y. Karpenkov, R. R. Gimaev, A. M. Chirkova,
A. Akiyama, T. Miyanaga, M. F. Hupalo, D. J. M. Aguiar, A. M.
G. Carvalho, G. F. Cabeza *et al.*, J. Alloy Comp. **898**, 163092 (2016).

[36] G. Shirane, R. Nathans, and C. W. Chen, Phys. Rev. **134**, A1547 (1964).

[37] G. Shirane, C. W. Chen, P. A. Flinn, and R. Nathans, Phys. Rev.
131, 183 (1963).

[38] T. Mochiku, Y. Matsushita, N. Subotić, T. Kashiwagi, and K. Kadowaki, Acta Cryst. **E77**, 1327 (2021).

[39] N. Subotić, T. Mochiku, Y. Matsushita, O. Takeuchi, T. Kashiwagi, H. Shigekawa, and K. Kadowaki, MRS Adv. **7**, 778 (2022).

[40] N. Subotić, T. Mochiku, Y. Matsushita, M. Nishio, O. Takeuchi, H. Shigekawa, and K. Kadowaki, MRS Adv. **8**, 404 (2023).

[41] H. Okamoto, T. B. Massalski, L. J. Swartzendruber, and P. A. Beck, Bull. Alloy Phase Diagr. **5**, 592 (1984).

[42] H. Okamoto and T. B. Massalski, Bull. Alloy Phase Diagr. **5**, 276 (1984).

[43] R. Barua, F. Jimenez-Villacorta, and L. H. Lewis, Appl. Phys. Lett. **103**, 102407 (2013).

[44] P. H. L. Walter, J. Appl. Phys. **35**, 938 (1964).

[45] J. A. Ricodeau and D. Melville, J. Phys. F: Met. Phys. **2**, 337 (1972).

[46] L. I. Vinokurova, A. V. Vlasov, N. I. Kulikov, and M. Pardavi- Horváth, J. Magn. Magn. Mater. **25**, 201 (1981).

C. J. Schinkel and R. Hartog, AIP Conf. Proc. **10**, 1365 (1973)

TABLE I. The composition of the melting experiments.

	Molar retios					
Melting experiment	Au	Fe	Pb	Rh	Batch	Quartz tube placement
A	2	2	4	1	A	Vertically
B	2	1	4	1	B_1, B_2	Horizontally
C	4	1	8	1	C_1, C_2	Horizontally

TABLE II. The results of EPMA measurement of FeRh single crystals are shown in Fig. 6. The number of measured points (N), the size, and the batch from where the crystals were taken are shown.

Sample No.	Fe	Rh	Size	N	Batch
1	50.1 ± 0.8%	49.9 ± 0.9%	100 × 100 × 1500 μm	10	B_2
2	50.4 ± 1.3%	49.6 ± 1.1%	120 × 120 × 700 μm	14	B_2
3	50.9 ± 1.1%	49.1 ± 1.1%	400 × 400 × 400 μm	13	B_2
4	49.6 ± 1.4%	50.4 ± 1.3%	200 × 300 × 10 μm	12	A

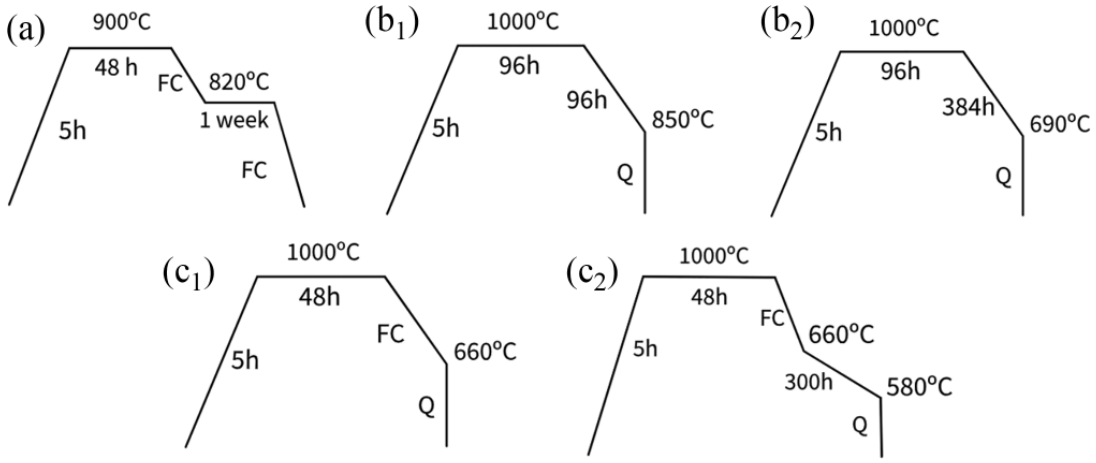

FIG. 1. The temperature profiles for the different batches. FC and Q stand for the furnace cooling and quenching processes, respectively.

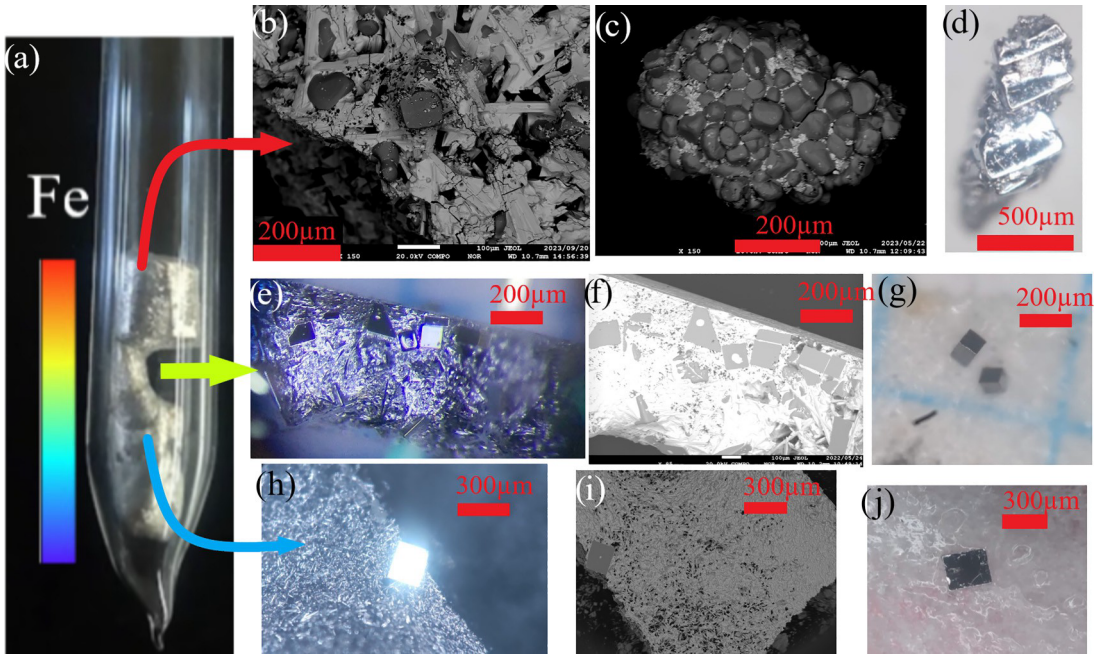

FIG. 2. Results of batch A. (a) The grown boule inside the quartz tube is shown. The color code represents the image of the Fe concentration [red means higher Fe concentration while blue means lower Fe concentration based on electron probe microanalyzer (EPMA) measurements]. In addition to the picture of the whole boule, the representative parts of the boule are shown: (b)–(d) are obtained from the upper part, (e)–(g) are obtained from the middle part, and (h)–(j) are obtained from the lower parts of the boule. As the Fe concentration decreases, the crystal habit becomes clearer due to the lower density of nucleation. The conglomeration growth (c) was often observed in the upper part of the boule, while crystals with clear shiny faces as seen in (e) and (h) in the rich AuPb flux part can be observed. Those crystals tend to precipitate to the surface as expected [40]. In the second column of the pictures, the EPMA composition images are shown, where the brighter parts correspond to AuPb flux, while the darker parts correspond to FeRh. The composition of FeRh is very close to the 1:1 ratio within the accuracy of ±1 at. %. In the far-right column, the extracted crystals are shown. The extraction of those crystals is relatively simple. The boule is immersed in diluted nitric acid (10%). Diluted nitric acid softens the AuPb flux from where, either mechanically or by vibration, the FeRh crystals can be separated.

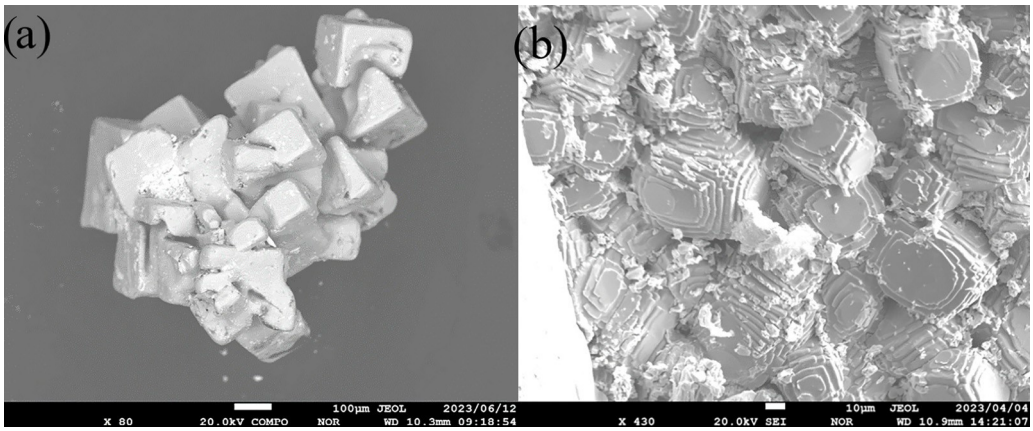

FIG. 3. Many small single crystals grown together at the upper part of the boule that is shown in Fig. 2. (a) The congregation of FeRh crystals. (b) Clear edges, steps, and terraces of FeRh crystals can be observed. The composition investigated by electron probe microanalyzer (EPMA) was Fe : Rh = 1:1 within an experimental error of ±1 at. %.

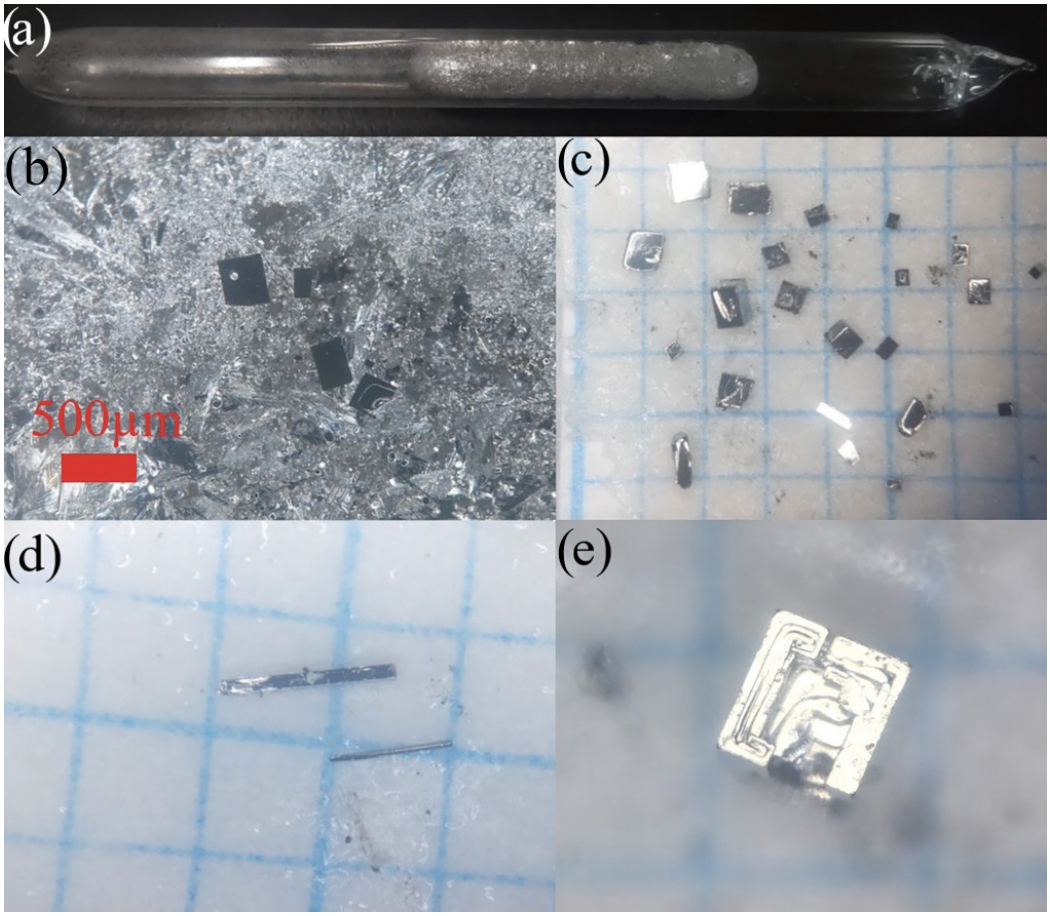

FIG. 4. The results of batch B_2. (a) The grown boule after the melting experiment. (b) One part of the surface of the boule. FeRh crystals with flat surfaces are clearly observed. Small shiny dots are found on the surface of FeRh crystals that have formed due to quenching. (c) Some of the FeRh crystals extracted from the surface of the boule. The surface of crystals is degraded if it is exposed to nitric acid for a longer time. (d) Needlelike crystals extracted from the inner part of the boule. (e) One of the hopper crystals of FeRh that usually forms at the bottom part of the boule. The underlying grid in the picture represents a 1 mm scale.

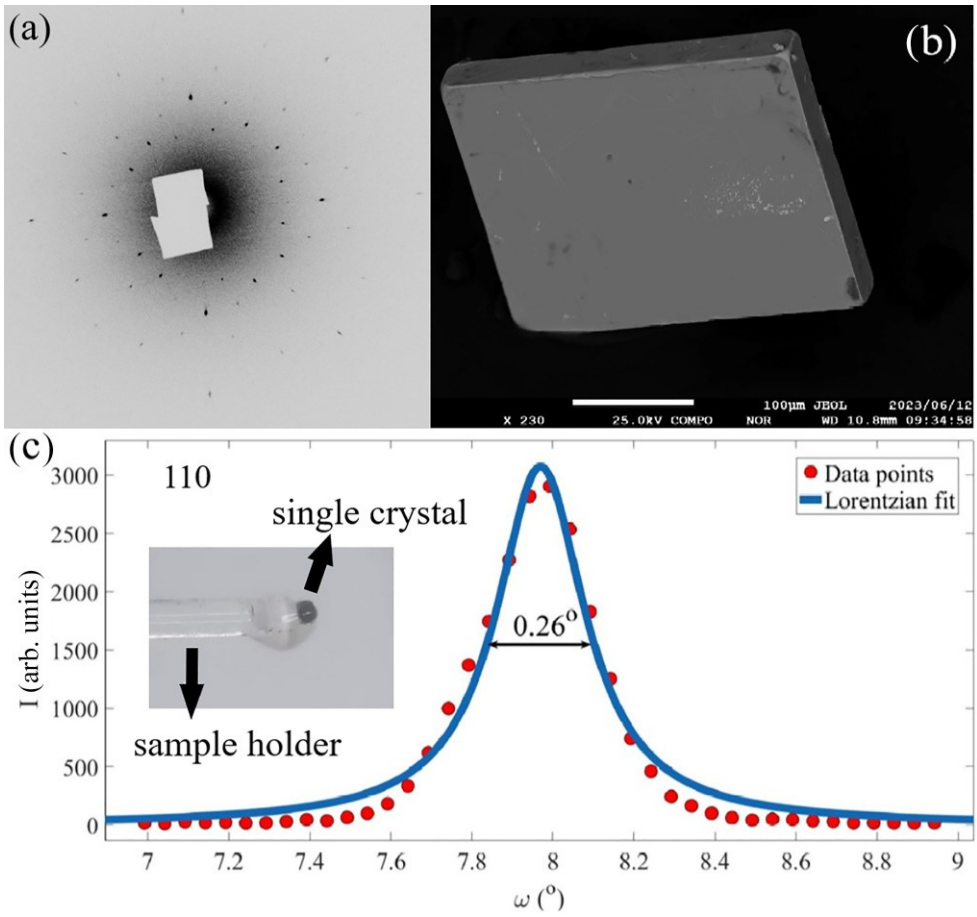

FIG. 5. The results of x-ray diffraction (XRD) analysis. (a) A typical photograph of the transmission Laue diffraction pattern ob- tained from the crystal shown in (b) using a W target (40 kV and 20 mA). The collimated x-ray beam was shone perpendicularly to the platelike single crystal of FeRh, and the imaging plate was put behind the single crystal ~5 cm apart from the crystal. (c) The ω scan rocking curve of the 110 reflection.

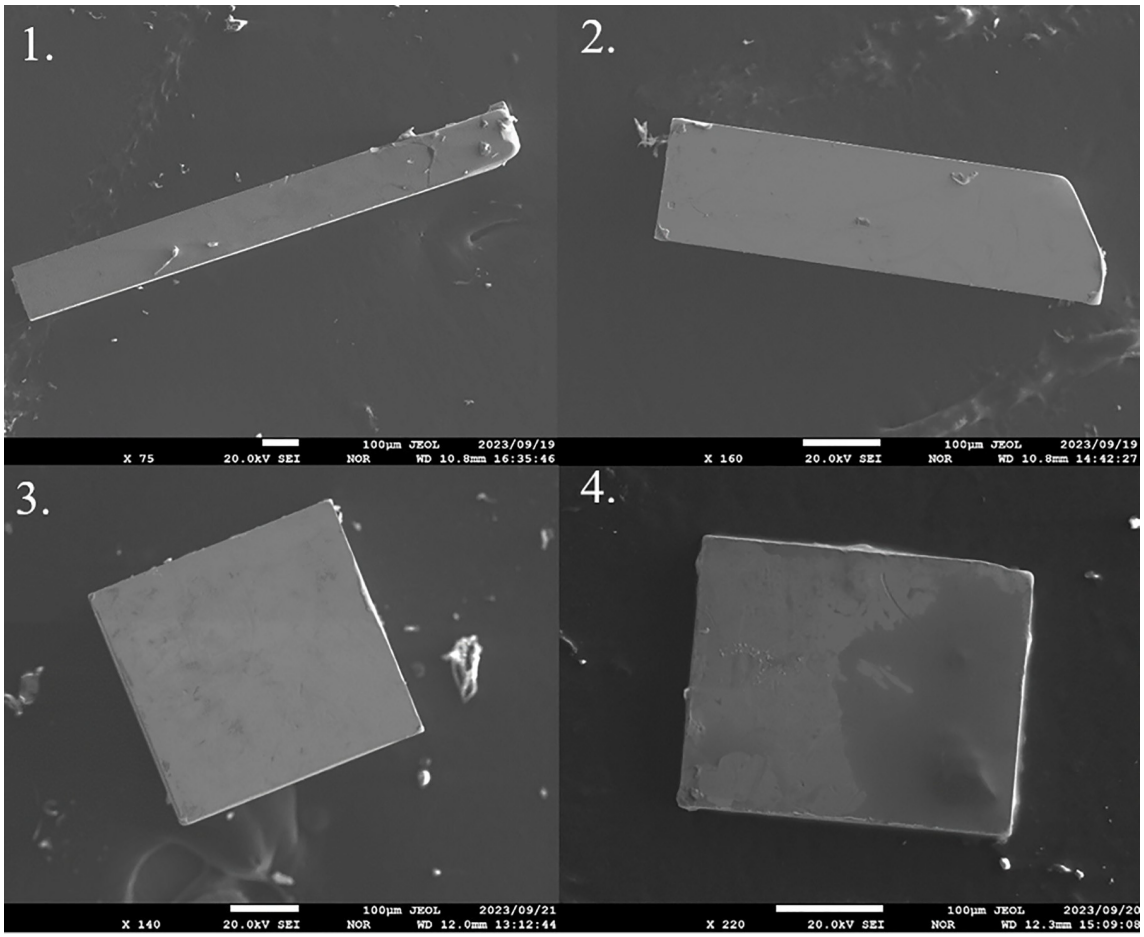

FIG. 6. The scanning electron microscopy (SEM) images of single crystals of FeRh on which electron probe microanalyzer (EPMA) measurements were done. Clear crystal habits with sharp edges can be observed. The scale in the photo (white bar shown in the lower part of the picture) represents 100 µm.

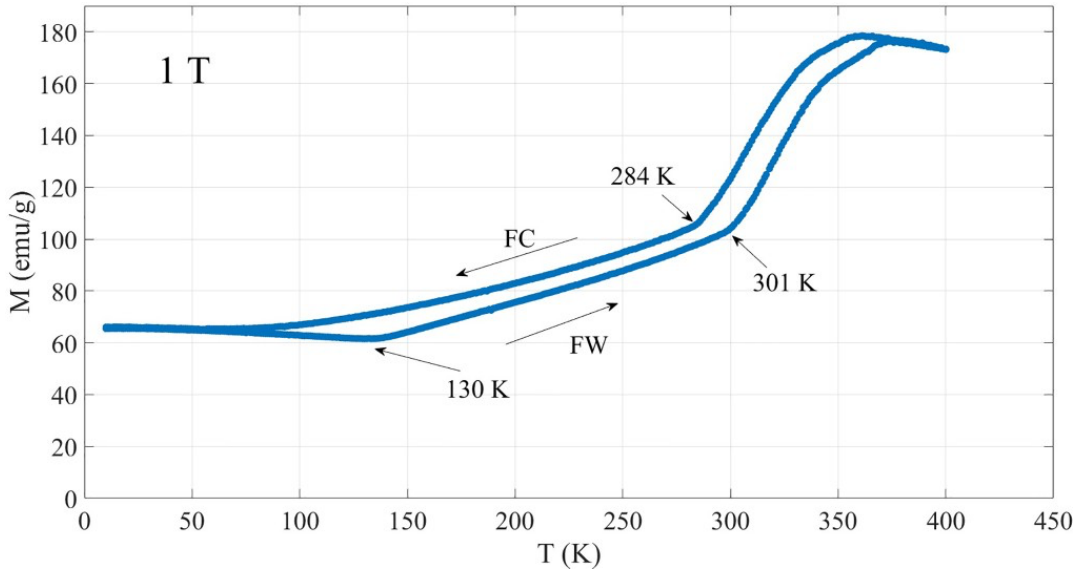

FIG. 7. Temperature dependence of magnetization $M(T)$ of FeRh in 1 T magnetic field applied to [1,0,0] direction between 10 and 400 K. The arrows denoted as FW and FC mean that the curves were obtained in the warming process and the cooling process, respectively.